Period doubling, Feigenbaum constant and time series prediction in an experimental chaotic RLD circuit

M.P. Hanias [a,*], Z. Avgerinos [b], G.S. Tombras [b]

[a] *Technological and Educational Institute of Chalkis, GR 34400, Evia, Chalkis, Greece*
[b] *Laboratory of Electronics, Department of Physics, University of Athens, Athens GR 15784, Greece*

Communicated by M.S. El Naschie

Abstract

An experimental setup of a chaotic resistor-inductor diode (RLD) circuit is presented. Following step-by-step its route to chaos through period doubling, Feigenbaum constant δ is calculated and its value is verified with noticeable accuracy. In addition, the analysis of the corresponding strange attractor shows that one- and multi-step prediction of the corresponding chaotic time series can be achieved in a real RLD circuit.
© 2007 Elsevier Ltd. All rights reserved.

1. Introduction

Chaos is the non-periodic behavior of deterministic nonlinear dynamic systems that is highly sensitive to initial conditions. Chaotic behavior can also be observed in a variety of presumably simple linear systems in which even a single parameter variation can lead to a behavior indicative of that of complex nonlinear systems, though governed by the same initial deterministic rules. Many electronic circuits are good examples of such systems and, in this respect, building a chaotic circuit can be of great help into understanding the mathematics and possible applications of this pervasive phenomenon. One of the routes to chaos is by period doubling or bifurcation [1–5]. According to this, when a sinusoidal signal of period 1 is applied to a system, its output will initially be equal to that of the input. However, if the value of a single parameter of the system is changed, the output period will bifurcate and if that value is changed again another bifurcation will occur and so on. Thus, as the parameter value changes, the output signal period becomes 2, 4, 8, 16, etc., and this continues until no more stable states are available. Interesting enough, for each new bifurcation, the amount of the parameter value need be changed decreases in a constant manner. By measuring the parameter's sequential changes and comparing each one to the next, a constant ratio called Feigenbaum's constant δ is yield [6–9]. A simple circuit that can exhibit such a chaotic behavior is the so-called RLD circuit, i.e. a series connection of a resistor R, an inductor L, and a junction diode D. The circuit is driven by a sinusoidal input voltage and the diode provides for the system's nonlinearity while its state-of-bias-related capacitance, combined with the inductance, gives the system the necessary degrees of freedom in order to produce chaos.

---

* Corresponding author.
 E-mail address: mhanias@teihal.gr (M.P. Hanias).

In this paper, we use a real RLD circuit and follow its route to chaos through period doubling. We consider this work in continuation of the recently presented time series analysis in simulated similar circuit, [10]. The remainder of the paper is organized as follows. In Section 2, we discuss on the RLD circuit setup and, in Section 3, we present the experimental procedure and the obtained results, from which, in Section 4, we calculate the Feigenbaum constant δ. In Section 5, we proceed to a one- and multi-step prediction of the corresponding chaotic time series. Concluding remarks are given in Section 6.

2. Description of the RLD circuit setup

The schematic diagram of the employed RLD circuit is shown in Fig. 1. The circuit consists of a simple inductor L, a diode D and a resistor R connected in series. Their values are $L = 4.88$ mH, $R = 100 \, \Omega$, and the diode type is IN4007. The input signal is a sinusoidal voltage v_s with frequency near or equal to the resonance frequency f_r of the circuit, while the voltage v_R across resistor R is considered to be the circuit output signal.

The resonance frequency of a series resistor, inductor, and capacitor (RLC) circuit is the signal frequency that corresponds to the maximum amplitude of the output voltage. Considering the diode's junction capacitance C_j, the resonance frequency f_r for the RLD circuit of Fig. 1 depends on this value. In this respect, f_r has been found to be approximately equal to 450 KHz by varying the input signal frequency until the output voltage takes its peak amplitude. Therefore, using the general expression:

$$f_r = \frac{1}{2\pi\sqrt{LC_j}} \tag{1}$$

the actual zero-biased dynamic junction capacitance of the diode [11], is found to be $C_j(0) = 25.63$ pF which is close enough to $C_j(0)_{IN4007} = 25.89$ pF given by the PSPICE model for IN4007.

In a RLD circuit, chaotic operation may eventually result due to the unrecombined electrons and holes that cross the forward-biased *pn* junction, and, as the diode changes state-of-bias, diffuse back to their origin [11]. Hence, the diode appears to act like a charging or discharging capacitor as its space-charge width varies accordingly. The larger the forward current, the greater the amount of charges that cross the junction and the longer the system needs to return to its reverse bias equilibrium. If the reverse current is unable to reach equilibrium before the forward bias, then the next cycle will depend upon the previous cycle, and, this will be equivalent to different parameters at each cycle's initial conditions. Thus, under such varying conditions, the circuit may become chaotic [11], and, this may be due to period doubling or bifurcation of the output signal [1,12].

Considering the operation of a system driven by a sinusoidal signal, its output signal power spectrum will contain the fundamental input frequency f_{IN} and some high order harmonics due to the system's nonlinearities. If the same system is to progress towards chaos by period doubling then additional frequency components, known as subharmonics and ultra-subharmonics, will appear [12–15]. However, for a truly chaotic system, there will be a spectrum of frequencies rather than specific peaks, while multiple "chaos" may also occur with broadening of the spectrum near certain frequencies.

When a RLD circuit is driven by an input signal with frequency near or equal to its resonance frequency f_r, the circuit may operate normally as expected [16]. If the input signal amplitude is increased, the operation will become unstable in the sense that the output signal periodic state will change and be divided into two frequency components dependent on f_r. The first component will be the harmonic but a second will also appear at half the harmonic. Further amplitude increase will result in splitting each new component, leading progressively into higher periodicity until there will be no more stable states available and chaos will prevail. This is exploited in the next section.
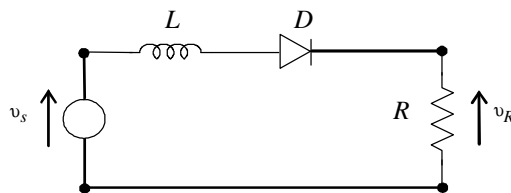
Fig. 1. The experimental RLD circuit.

3. Experimental procedure and results

In the considered RLD circuit, the input signal frequency f_{IN} is set equal to f_r, i.e. $f_{IN} = f_r = 450$ KHz, and remains unchanged as its amplitude is increased. A two-channel oscillator is used in order to monitor the variations of input and output signals, and, most importantly, the resulting loops when set in X–Y mode. Hence, before the first period doubling there will be a single loop, while afterwards there will be two loops, four, etc. A spectrum analyzer is also used to monitor the output signal frequency spectrum. This is particularly helpful in clarifying the occurrence of each bifurcation and measure the value of any new frequency peak that appears on screen.

We now describe step-by-step the experimental procedure that leads the RLD circuit of Fig. 1 to chaotic behavior. At first, the input signal amplitude is increased to a peak-to-peak value $V_{pp} = 1.11$ V. As shown in Fig. 2a–c, the output signal remains sinusoidal and only one loop appears in X–Y mode. However, Fig. 2d shows that a small frequency peak appears at 900 KHz being the first harmonic of the input signal fundamental frequency and a typical consequence of the RLD circuit nonlinearity.

In a second step, V_{pp} is firstly increased up to $V_{pp} = 1.14$ V, where, as shown in Fig. 3, a first period doubling occurs with a subharmonic frequency peak at 225 KHz and an ultra-subharmonic peak that is just about to appear at around 675 KHz indicating the first bifurcation of the fundamental input frequency of 450 KHz.

After that, V_{pp} is increased up to $V_{pp} = 1.62$ V, where, as shown in Fig. 4, a second period doubling occurs, three loops appear in X–Y mode, the 675 KHz ultra-subharmonic is clearly shown and the second period doubling is indicated with the just to appear frequency peaks at around 112.5 KHz and 337.5 KHz.

In Fig. 5, V_{pp} is increased to $V_{pp} = 1.74$ V and the occurring new bifurcation results into a total of seven loops and seven distinguishable frequency peaks.

Following that, a new increase of the input signal amplitude leads to chaos. This is shown in Fig. 6, while along with Fig. 7, it can be seen that as the input amplitude is further increased, the output chaos will accordingly be strengthened. However, it must not be overlooked that this is limited by the fact that chaos will be eventually destroyed [17,18].

4. Feigenbaum constant calculation

Feigenbaum's constant δ can be experimentally calculated according to the expression [12,16,19,20]:

$$\delta = \frac{P_{n+1} - P_n}{P_{n+2} - P_{n+1}} \tag{2}$$
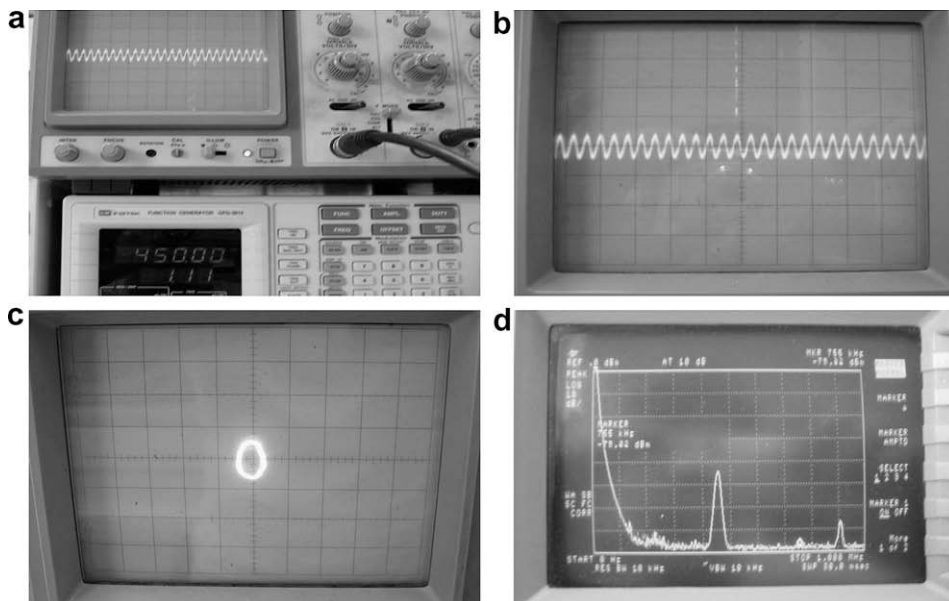
Fig. 2. (a) Input signal generator settings and output signal v_R, (b) v_R waveform before any period doubling. (c) X–Y mode: only one loop, (d) spectrum analyzer display of the fundamental frequency component at 450 KHz and its first harmonic at 900 KHz.
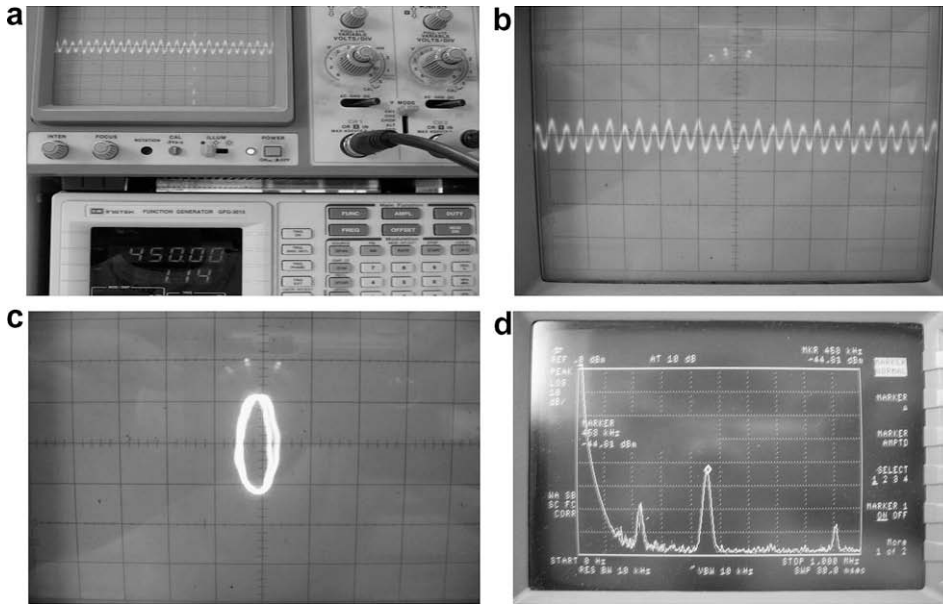
Fig. 3. (a) Input signal generator settings and output signal v_R, (b) v_R waveform after the first period doubling, (c) X–Y mode: a second loop just appears indicating the first period doubling, (d) display of the first period doubling with the first subharmonic at 225 KHz along with an indication that an ultra-subharmonic will appear at 675 KHz.
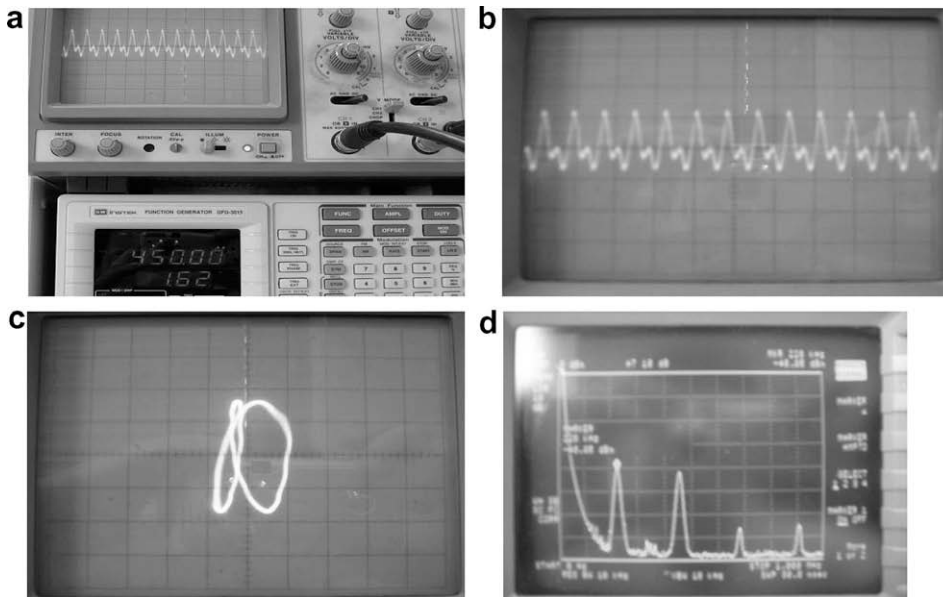
Fig. 4. (a) Input signal generator settings and output signal v_R, (b) v_R waveform after the 2nd period doubling, (c) X–Y mode: three loops can be seen, (d) three clear frequency peaks at 225, 450, and 675 KHz (left-to-right) and two peaks at 112.5 and 337.5 KHz just before to appear (the harmonic at 900 KHz is irrelevant and thus excluded).

where P_n is the value of the changing parameter, i.e. the driving input voltage amplitude, in one bifurcation, and P_{n+1}, P_{n+2} the corresponding parameter values for the next two bifurcations. Following that, the obtained values are summarized in Table 1 and lead to:
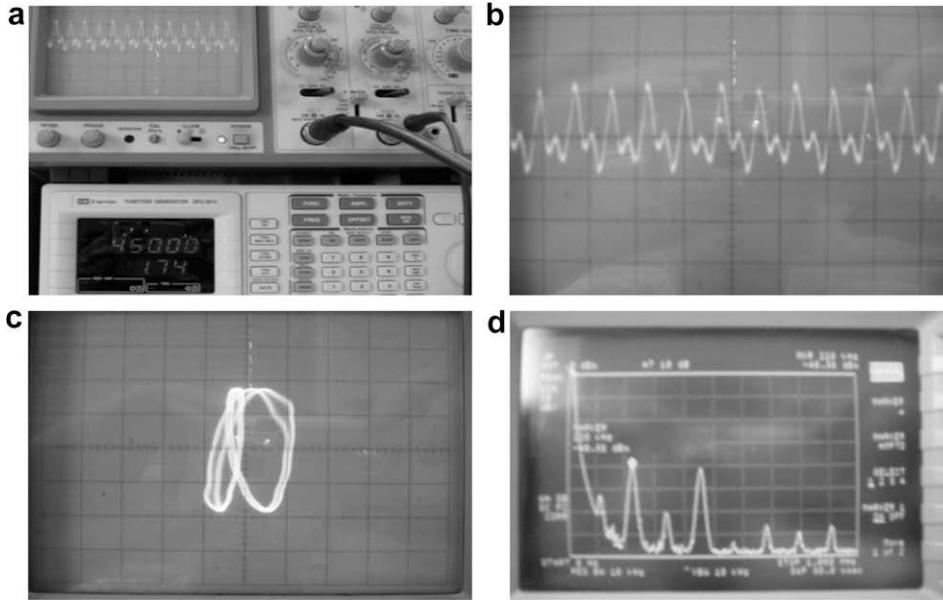
Fig. 5. (a) Input signal generator settings and output signal v_R, (b) v_R waveform after the first period doubling, (c) X–Y mode: seven loops are present, (d) spectrum analyzer display: seven frequency peaks at 112.5, 225, 337.5, 450, 562.5, 675, and 787.5 KHz (the harmonic at 900 KHz is excluded).
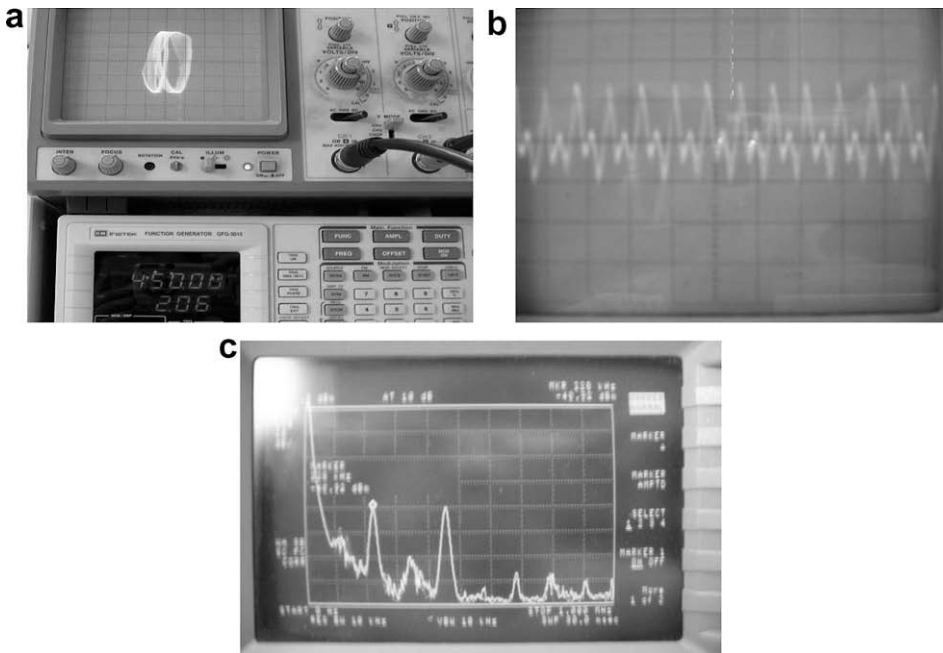
Fig. 6. (a) Input signal generator settings and X–Y mode loops, (b) v_R chaotic waveform, (c) spectrum analyzer display of the obtained chaos.

$$\delta = \frac{1.62 - 1.11}{1.74 - 1.62} = 4.25 \tag{3}$$

which is a mere 8.97% decline in comparison to the theoretical value $\delta = 4.669$ [11,16] due to experimental faults, and, thus, it is well acceptable.
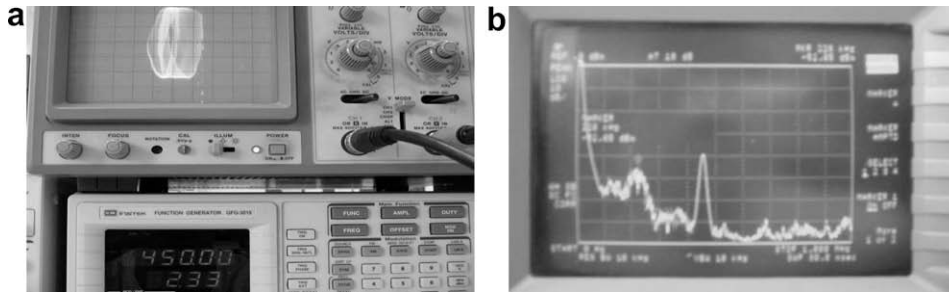
Fig. 7. (a) Input signal generator settings and *X–Y* mode loops. (b) Spectrum analyzer display of the RLT chaotic behavior.

Table 1
Survey of results of period doubling and chaos on RLD circuit with different values of input amplitude and the corresponding transitions

V_{pp} (V)	Period
1.11	Transition 1–2
1.62	Transition 2–4
1.74	Transition 4–8

5. Time series prediction

In this section, we consider the RLD circuit with input amplitude $V_0 = 890$ mV ($V_{pp} = 1.78$ V) and use a reordered time series in order to predict the voltage $V = vR(t)$ across R. In particular, we use local models to predict the one step and the multi-step procedures. That is, instead of fitting one complex model with many coefficients to the entire data set, we fit many simple models (low order polynomials) to small portion of the data set depending on the geometry of the local neighbourhood of the dynamical system [21,22]. The general procedure is the following: to predict point V_{i+1}, we determine the last known state of the system as represented by vector $\mathbf{X} = [\mathbf{V_i}, \mathbf{V_{i-\tau}}, \mathbf{V_{i-2\tau}}, \mathbf{V_{i-(m-1)\tau}}]$, where m is the embedding dimension and τ is the time delay as determined by the first minimum of the average mutual information function I_{av}, i.e. $\tau = it$ where $i = 1, \ldots, N$, [23–26]. Here, keeping in mind that the sample rate is $t = 0.222$ ns, the average mutual information I_{av} exhibits a local minimum at $\tau = 34$ time steps, as shown in Fig. 8. Thus, we use as a delay time equal to $\tau = 34$.

According to Taken, [27,28], an m dimensional delay vector will be embedded with a minimum embedding dimension m when $m \geqslant 2v + 1$ with v being the correlation dimension. In other words, Takens' embedding theorem asserts that if the attractor dimension is v, then for a complete understanding of the attractor, $2v + 1$ dimensions in the embedding space will be sufficient. Further generalization asserts that any embedding dimension larger than the correlation dimension will be sufficient for a complete characterization of the attractor, [29,30]. Moreover, the minimum embedding dimension will be the smallest integer greater than the correlation dimension. Following [10], the correlation dimension for an RLD circuit has been found equal to $v = 2.11$.

Hence, considering as optimum the values of delay time $\tau = 34$ and embedding dimension $m = 3$, we then search the time series to find k similar states that have occurred in the past, where "similarity" is determined by evaluating the distance between vector $\mathbf{X}$ and its neighbour vector $\mathbf{X}'$ in the m-dimensional state space. Thus, k close states of the system that have occurred in the past are found by computing their distances from $\mathbf{X}$ and usually these are the k nearest neighbours of $\mathbf{X}$. The idea, here, is to fit a map which extrapolates $\mathbf{X}$ and its k nearest neighbours to determine the next value. If the observable signal was generated by some deterministic map $M(V_i, V_{i-\tau}, V_{i-2\tau}, V_{i-(m-1)\tau}) = V_{i+\tau}$, that map could be recovered (reconstructed) from the data by simply looking at its behavior in the neighbourhood of $\mathbf{X}$. Using this map, an approximate value of V_{i+1} will then be obtainable.

We find the approximation of M by fitting a (low order) polynomial which maps the k nearest neighbours (similar states) of $\mathbf{X}$ onto their next immediate values. We use a fixed size of nearest neighbours $k = 7$ and then use this map to predict V_{i+1}. In other words, we assume that M is fairly smooth around $\mathbf{X}$, and so if a state $\mathbf{X}' = [\mathbf{V'_i}, \mathbf{V'_{i-\tau}}, \mathbf{V'_{i-2\tau d}}, \mathbf{V'_{i-(m-1)\tau}}]$ in the neighbourhood of $\mathbf{X}$ resulted in the observation V'_{i+1} in the past, then the point V_{i+1} which we want to predict must be somewhere near V'_{i+1}, [21].
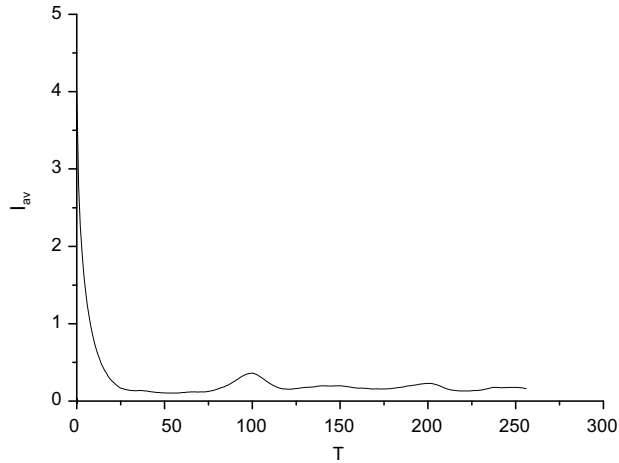
Fig. 8. Average mutual information I_{av} vs. time delay τ.

We use both the one step and multi-step ahead prediction methods. In the one step ahead prediction, after each step in the future is predicted, the actual value is utilized for the next one step prediction. In contrast, the multi-step prediction is based only on the initial k states. The calculated performance is otherwise known as the normalized mean squared error (NMSE) and calculated by,

$$\text{NMSE} = \text{MAX}\left[\frac{\sum_{i=1}^{NP}(\widetilde{V}_i - V_i)^2}{\sum_{i=1}^{NP}(\overline{V}_i - V_i)^2}, \frac{\sum_{i=1}^{NP}(\widetilde{V}_i - V_i)^2}{\sum_{i=1}^{NP}(V_{i-1} - V_i)^2}\right] \tag{4}$$

where $\widetilde{V}_i$ is the predicted value, V_i is the actual value, $\overline{V}$ is the average actual value, and NP is the range of values in the prediction interval. From Eq. (4) it can be seen that NMSE is the mean squared error of our predictor normalized by the mean squared error of a random walk predictor. By definition, the minimum value of NMSE is 0. At that value there is an exact match between the actual and the predicted values. The higher NMSE, the worse is our prediction as compared to the trivial predictors. If NMSE is equal to 1, our prediction is as good as the prediction by the trivial predictor. If NMSE is greater than 1, our prediction is worse. Using $\tau = 34$ and $m = 3,4$ or 5, we find that optimum values are $\tau = 34$ and $m = 5$, $k = 7$ for which the minimum NMSE is achieved. We use the locally weight linear predictor method for predicting one step ahead the voltage $V = v_R$ across R. In addition, in order to determine a weighting
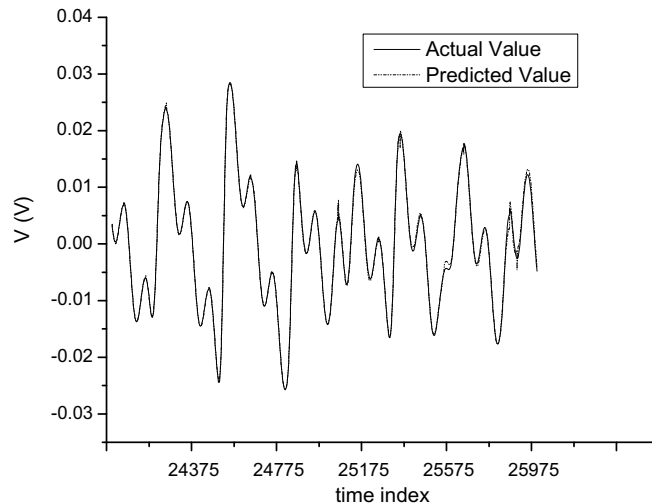
Fig. 9. One step prediction of voltage oscillations across the resistor.
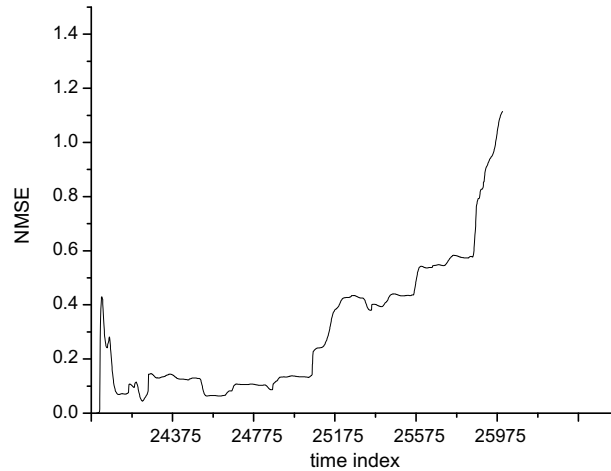
Fig. 10. Mean squared error of our predictor normalized by the mean squared error of the random walk predictor for one step prediction.
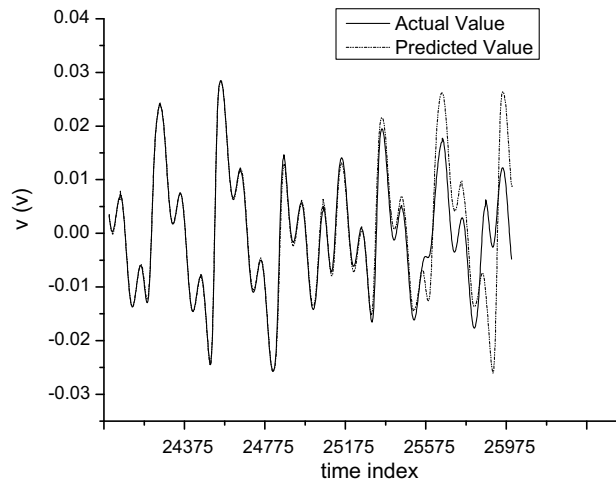
Fig. 11. Multi-step prediction of voltage oscillations across the resistor.

function to assign the contribution of each neighbour to our locally weighted linear predictor, we use the tricube Kernel [30–33]:

$$K(d,h) = \left[1 - \left(\frac{d}{h} \right)^3 \right]^3 \qquad (5)$$

where d is the Euclidean distance between vectors $\mathbf{X}$ and $\mathbf{X}'$ at a phase space with dimension $m = 5$ and h is the bandwidth of the neighbourhood formed by $k = 7$ neighbours and weights the contribution of each of the $k = 7$ nearest neighbours of the reference state $\mathbf{X}$ to the resulting prediction. Furthermore, this bandwidth controls the size of the neighbourhood in which the nearest neighbours are sought.

In our predictor the bandwidth is implemented as a variable bandwidth [21,34] where the actual number indicates the number of the nearest neighbours of the reference state to search. Once that number is set, the size of the neighbourhood will change in the process of training to include the exact number of the neighbours specified. That is, the neighbourhood will be larger (resp. smaller) in the sparse (resp. dense) regions of the attractor. In general, the larger is the bandwidth, the lower is the variance and the greater is the bias of the predictor. For the very low values of band-
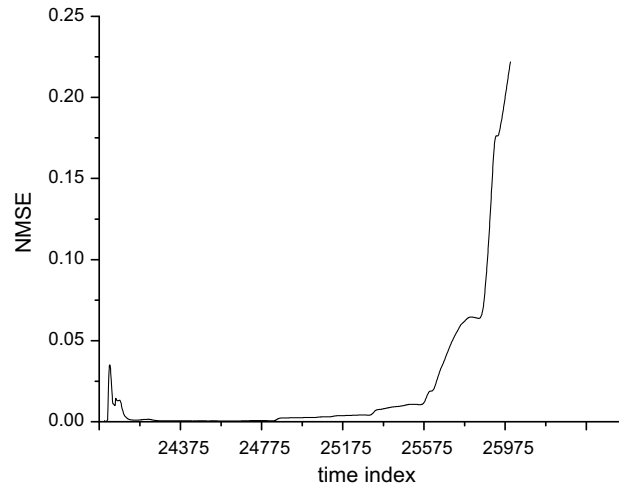
Fig. 12. Mean squared error of our predictor normalized by the mean squared error of the random walk predictor for multi-step prediction.

width, the predictor simply interpolates between points, while for the very large values of bandwidth, the local predictor becomes a global one since it considers all the points in the data set. Then, the contribution of each neighbour to the regression is calculated according to Eq. (5). In the present analysis, we used 26,000 data points and predicted the evolution for 2000 succeeding dimensionless time steps from 24,000 to 26,000. We then computed the NMRSE as the Root mean square error of the prediction as well. The obtained results are shown in Fig. 9 where the one step ahead predicted values are coming from an out-of-sample set prediction, where we pretend that we know the data only up until this point, and we try to predict from there, while the one step ahead predicted values are coming from prediction out-of-sample set. The NMSE is then shown in Fig. 10 for the one step prediction. The root mean square error (RMSE) for this prediction is found equal to 0.000473.

Finally, we use the same procedure as before but with multi-step ahead predictions and the results are shown in Fig. 11. Respectively, Fig. 12 depicts NMSE for multi-step prediction while the corresponding RMSE is found equal to 0.005145.

6. Conclusion

With a resistor, diode and inductor in series and a sinusoidal drive signal, we were able to experimentally drive a circuit into chaos. Our circuit recapitulated the Feigenbaum universal constant and the calculated value proved to be close enough to the theoretically expected value. Furthermore, using as input parameters the invariant parameters that characterize the strange attractor, we achieved both one step and multi-step prediction of the corresponding chaotic time series that governs the dynamics of the considered RLD circuit.

References

[1] Alligood KI, Sauer TD, Yorke JA. Chaos: An introduction to dynamical systems. New York: Springer; 1996.
[2] Cooper C. Chaos, Solitons & Fractals 2005;24:157–63.
[3] Wang L, Xu M. Chaos, Solitons & Fractals 2005;24(2):527–32.
[4] Luo ACJ. Chaos, Solitons & Fractals 2004;19(4):823–39.
[5] Stavrinides SG, Kyritsi KG, Deliolanis NC, Anagnostopoulos AN, Tamasevicious A, Cenys A. Chaos, Solitons & Fractals 2004;20(4):843–7.
[6] Feigenbaum MJ. Universal behavior in nonlinear systems. Los Alamos Science 1980;1:4–27.
[7] Goldfain E. Chaos, Solitons & Fractals 2006;30(2):324–31.
[8] San Martin J. Chaos, Solitons & Fractals 2007;32(2):816–31.
[9] Letellier C, Bennoud M, Martel G. Chaos, Solitons & Fractals 2007;33(3):782–94.

[10] Hanias MP, Giannaris G, Spyridakis A, Rigas A. Chaos, Solitons & Fractals 2006;27(2):569–73.
[11] Mariz de Moraes R, Anlage SM. Phys Rev E 2003;68:026201.
[12] Enns R, McGuire G. Nonlinear physics with mathematica for scientists and engineers. Boston: Birhkauser; 2001.
[13] Yang J, Feng W, Jing Z. Chaos, Solitons & Fractals 2006;30(1):235–56.
[14] Cafagna D, Grassi G. Chaos, Solitons & Fractals 2005;25(2):499–507.
[15] Jing Z, Wang R. Chaos, Solitons & Fractals 2005;23(2):399–411.
[16] Carroll TL, Pecora LM. Phys Rev E 2002;66:046219.
[17] Kaplan D, Glass L. Understanding nonlinear dynamics. New York: Springer-Verlag; 1995.
[18] Hilborn RC. Chaos and nonlinear dynamics. New York: Oxford University Press; 1994.
[19] Linz SJ, Sprott JC. Elementary chaotic flows. Phys Lett A 1999;259:240–5.
[20] Peitgen H-O, Jurgens H, Saupe D. Fractals for the Classroom. New York: Springer-Verlag, New York Inc.; 1992.
[21] Kononov E. Virtual Recurrence Analysis 2006;4(9) [email:eugenek@ix.net.com.com].
[22] Ryabov VB, Correig AM, Urquizu M, Zaikin AA. Chaos, Solitons & Fractals 2003;16(2):195–210.
[23] Kantz H, Schreiber T. Nonlinear time series analysis. Cambridge University Press; 1997.
[24] Aasen T, Kugiumtzis D, Nordahl SHG. Comput Biomed Res 1997;30:95–116.
[25] Fraser AM, Swinney HL. Phys Rev A 1986;33:1134.
[26] Fraser AM. IEEE Trans Inf Theory 1989;35:245.
[27] Takens F. Detecting strange attractors in turbulence, Lecture notes in mathematics, 898. In: Rand DA, Young LS, editors. Berlin: Springer; 1981. p. 366–81.
[28] Miliou AN, Valaristos AP, Stavrinides SG, Kyritsi K, Anagnostopoulos AN. Chaos, Solitons & Fractals 2007;33(4):1248–55.
[29] Sauer T, Yorke J. Ergod Theory Dyn Syst 1997;17:941.
[30] Sauer T, Yorke J. Int J Bifurcation Chaos Appl Sci Eng 1993;3:737.
[31] Cleveland WS, Devlin SJ. J Am Stat Asso 1988;83:596–610.
[32] Wang Z, Isaksson T, Kowalski BR. Anal Chem 1994;66(2):249–60.
[33] Erfanian Omidvar A. Chaos, Solitons & Fractals 2004;22(4):757–66.
[34] Babinec P, Jakubikova E, Leszczynski J. Chaos, Solitons & Fractals 2004;21(2):513–4.